Natural Hazards
https://doi.org/10.1007/s11069-024-06487-3

ORIGINAL PAPER

Understanding fatal landslides at global scales: a summary of topographic, climatic, and anthropogenic perspectives

Seçkin Fidan[1,2] · Hakan Tanyaş[3] · Abdullah Akbaş[4] · Luigi Lombardo[3] · David N. Petley[5] · Tolga Görüm[2]

Received: 4 November 2023 / Accepted: 29 January 2024

Abstract

Landslides are a common global geohazard that lead to substantial loss of life and socio-economic damage. Landslides are becoming more common due to extreme weather events and the impacts of anthropogenic disturbance, and thus, they are threatening sustainable development in many vulnerable areas. Previous studies on fatal landslides have focused on inventory development; spatial and temporal distributions; the role of precipitation or seismic forcing; and human impacts. However, climatologic, topographic, and anthropogenic variables featuring fatal landslides at a global scale have been mostly neglected. Here, using the global fatal landslide database, we evaluate the characteristics of landslides induced by natural and anthropogenic factors with respect to topographic, climatic, and anthropogenic factors, drawing attention to their persistent spatial patterns. The majority of natural (69.3%) and anthropogenic (44.1%) landslides occur in mountainous areas in tropical and temperate regions, which are also characterized by the highest casualty rates per group, 66.7% and 43.0%, respectively. However, they significantly differ in terms of their morphometric footprint. Fatal landslides triggered by natural variables occur mostly in the highest portions of the topographic profile, where human disturbance is minimal. As for their anthropogenic counterpart, these failures cluster at much lower altitudes, where slopes are gentler, but human intervention is higher due to a higher population density. This observation points towards land cover changes being a critical factor in landscape dynamics, stressing the human pressure as a discriminant cause/effect term for natural vs. human-induced landslide fatalities.

Keywords Bivariate · Landslide · Fatality · Fatal landslide · Spatiotemporal persistence

✉ Seçkin Fidan
seckinfidan@ankara.edu.tr

[1] Department of Architecture and Urban Planning, Ankara University, Ankara, Turkey

[2] Eurasia Institute of Earth Sciences, Istanbul Technical University, Istanbul, Turkey

[3] Faculty of Geo-Information Science and Earth Observation (ITC), University of Twente, Enschede, The Netherlands

[4] Department of Geography, Faculty of Arts and Science, Bursa Uludag University, Bursa, Turkey

[5] University of Hull, Hull HU6 7RX, UK

Published online: 27 February 2024

1 Introduction

Landslides are one of the most widespread geohazards that globally cause significant loss of life and environmental damage (Petley 2012; Kirschbaum et al. 2015; Froude and Petley 2018). Impacts of landsliding are exacerbated by more frequently occurring extreme weather events and increased human occupation of vulnerable mountainous landscapes (Grima et al. 2020). Specifically, the growing demographic pressure and land use/cover changes are expected to increase the frequency and impacts of landslides in both rural (Guns and Vanacker 2014; Froude and Petley 2018; Maki Mateso et al. 2023) and urban (Gariano and Guzzetti 2016; Froude and Petley 2018; Ozturk et al. 2022) areas.

Therefore, developing a better understanding of variables controlling landslide occurrence is a critical element in landslide disaster prevention. In this context, the recording, monitoring, and analysis of landslides form essential elements in developing more robust predictive models.

Digital documentation and archiving of landslides have become increasingly common, most notably in the last two decades (e.g., Tanyaş et al. 2017; Emberson et al. 2022). Despite the expanding literature, financial losses and fatalities are rarely reported as part of landslide event inventories. And yet, a relatively large literature has been constructed that targets climatic and anthropogenic influences on fatal landslides across different spatial and temporal domains, including national (e.g., Petley et al. 2007; Lin and Wang 2018; Görüm and Fidan 2021; Garcia-Delgado et al. 2022), regional (e.g., Petley 2010; Sepúlveda and Petley 2015; Haque et al. 2016, 2019), and global (e.g., Kirschbaum et al. 2010, 2015; Petley 2012; Froude and Petley 2018; Haque et al. 2019) scale assessments.

The contextual effect of human stress on slopes under extreme weather conditions has already been noticed in a number of global studies, emphasizing hotspots in Central and Southeast Asia; Central and South America; as well as East Africa (Kirschbaum et al. 2012, 2015; Froude and Petley 2018; Haque et al. 2019). Such occurrences have also been responsible for a proportional increase in fatalities (Haque et al. 2019). A closer look at fatal landslide hotspots highlights South Asia as the most affected region, mainly driven by the summer monsoon, and East Asia, driven by landfalling tropical cyclones and a monsoonal climate. These aspects have been explored in depth by Petley (2010), which also highlights Southeast Asia (mainly the Philippines and Indonesia) as a landslide fatality hotspot, albeit without linking them to a specific climatic regime. Similar studies have also been conducted in other parts of the world. Sepúlveda and Petley (2015) examine fatalities in the Caribbean region, Central America, Colombia, and southeastern Brazil. They emphasize the role of large-scale hurricanes, with the El Niño/La Niña cycle as an additional disturbance, potentially leading to more fatalities. In another study focusing on the European landscape, Haque et al. (2016) argue that human activities may exert a minor effect with respect to extreme natural agents.

Similar studies have also been carried out at finer spatial scales, being tailored to specific countries such as the Democratic Republic of Congo (Depicker et al. 2021), Nepal (Petley et al. 2007), and Turkey (Görüm and Fidan 2021), where the spatial distribution of landslides has been associated with land use changes, civil wars or economic and political influences, respectively. This implies that anthropogenic influences seem to be more apparent in a finer resolution review. For instance, Garcia-Delgado et al. (2022) refer to low income, high corruption, and inequality effects as factors increasing the vulnerability against landsliding in Colombia.

This overall perspective on such a complex phenomenon has lacked a holistic examination of how macro-landforms and their morphometric characteristics, anthropogenic pressure, and climatic regimes interplay to generate landslide-related losses. The research reported here aims to start to fill this specific gap. With this idea in mind, we accessed the Global Fatal Landslide Database (GFLD) produced by Froude and Petley (2018) and initially aggregated the records at the basin scale. Then, we examined the persistent spatio-temporal occurrence of landslide fatalities against a number of morphologic and climatic features, aiming at capturing variations between landslides driven by natural or anthropogenic variables.

2 Data

In this study, we selected a total of 12 potential controlling factors in five categories: topographic (elevation, slope, elevation standard deviation, compound topographic index, and macro landforms), climatic (climate classification and precipitation), hydrographic (sub-basins), economic (GDP per capita) and anthropogenic (population, human footprint, and land cover change) variables from a variety digital sources (Table 1).

2.1 Landslide data

We used the GFLD information collected from 2004 to 2017 (Froude and Petley 2018), which exclusively reports fatal landslides triggered by non-seismic causes, such as precipitation and human activities. The GFLD compiles landslide records in news reports, scientific studies, and government reports. In addition, the database provides information about location and associated accuracy, occurrence date, type, cause, and number of victims. Also, the location accuracy in GFLD is addressed based on administrative units such as villages or states. To carry out the assessment in this manuscript, we selected all fatal landslides with a location accuracy of 10 km or less. Such a level of accuracy is suited to a global scale analysis, particularly because the data aggregation (presented in the following Sections) has been performed over catchments with a mean planimetric extent of 130 km^2 and a variation of 69 km^2 measured in one standard deviation.

2.2 Economic data

Most landslide-related deaths and economic damage are clustered in urban areas and specifically in countries with low GDP per capita (Froude and Petley 2018). In low to middle-income countries, fatal landslides are more frequent on slopes where people live in shanty towns (Alexander 2005; Sepúlveda and Petley 2015). In this overall scenario, if we were to include high-income countries in the analysis—for instance, with a 2017 GDP per capita (World Bank 2017) of more than $20,000—the results would potentially be biased. Therefore, we excluded nations fulfilling the above criterion and focused on the fatal landslide information about low- and middle-income countries.

2.3 Hydrography data

To eliminate the effect of uncertainty regarding the point representation of landslides, we spatially represented landslides at the basin scale, making use of the HydroBASINS

Table 1 The list of datasets used in this research

Data category	Data type	Datasets	Resolution	Source and details
Landslide	Fatal landslide	Global Fatal Landslide Database (GFLD)	Variable (location accuracy < 10 km)	Froude and Petley (2018)
Economic	GDP Per Capita	World Bank national accounts data and OECD National Accounts data files	Country-based	World Bank (2017)
Hydrography	Sub-basins	HydroBASINS	15 arcsecond (~ 450 m)	Lehner and Grill (2013)
Topographic	Elevation	MERIT DEM	3 arcseconds (~ 90 m)	Yamazaki et al. (2017)
	Elevation standard deviation (elev-std)	Geomorpho90m	90 m	Amatulli et al. (2020)
	Slope	Geomorpho90m	90 m	Amatulli et al. (2020)
	Compound topographic index (CTI)	Geomorpho90m	90 m	Amatulli et al. (2020)
	Macro landform	Macro Landform	30′ × 30′ (~ 55 km)	Amatulli et al. (2020)
Climatological	Köppen-Geiger climate classification	Köppen-Geiger	1 km	Beck et al. (2018)
	Precipitation	CHELSA Bioclim	30 arcsecond (~ 1 km)	Karger et al. (2017)
Anthropogenic	Population density	LandScan Global Population Distribution Dataset	1 km	Bright et al. (2004, 2017); Bright and Coleman (2001, 2003); Rose et al. (2018, 2021)
	Human footprint (H.F.)	Human Footprint	1 km	Mu et al. (2022)
	Land cover (only forest and settlement)	Copernicus Climate Change Service (C3S), Climate Data Store (CDS)	300 m	Climate Data Store (2019)

dataset. This dataset was created from hydrologically corrected DEMs (~30 m), and fed to a flow path routing method. The resulting hydrological basins were computed and stored across different spatial scales. These correspond to 12 levels of hierarchically nested global sub-basins (Lehner and Grill 2013). In the remainder of the manuscript, all analyses refer to the 12th level.

2.4 Topographic data

We used the MERIT-Digital Elevation Model (DEM) created by Yamazaki et al. (2017) as the baseline elevation data for topographic analysis. MERIT DEM is a worldwide terrain elevation dataset with a 3-arcsecond resolution (~90 m at the equator) that covers land regions between 90N-60S concerning the EGM96 geoid. The high-accuracy global MERIT DEM was developed by removing multiple errors, including absolute bias, stripe noise, speckle noise, and tree height bias. For other topographic parameters associated with landslides, we used the Geomorpho90m global dataset, which consists of different geomorphometric features also derived from the MERIT DEM (Amatulli et al. 2020). These features correspond to slope, elevation standard deviation (elev-std), and compound topographic index, and their use as part of our analyses will be described in the data pre-processing section.

To further characterize catchment characteristics associated with fatal landslide information, we also used a macro-landform description (Meybeck et al. 2001) aggregated into five diagnostic classes: (1) plains, (2) lowlands, (3) platforms, (4) plateaus, and (5) mountains.

2.5 Climatological data

For climate analyses, we used the 1 km resolution Köppen-Geiger climate classification of Beck et al. (2018). The authors group the world's climates into five main classes: (A) tropical, (B) arid, (C) temperate, (D) continental, and (E) polar. To this generic description, we added a more precipitation-oriented one, using the CHELSA v2.1 climate dataset (Karger et al. 2017, 2021). This dataset is expressed at a 30-arcsecond (~1 km) spatial resolution, and from it, we extracted the mean annual precipitation layer (i.e., BIO12) over the last 30 years (1981–2010).

2.6 Anthropogenic data

To examine the role of anthropogenic factors, we used three different proxies. First, we used global population data from 2000 to 2020. Because the GFLD dataset has both spatial and temporal dimensions, we extracted the information related to the population for the period when the fatal landslide occurred. The population data was accessed through the LandScan Global Population Distribution Dataset, a 1 km resolution product (Bright et al. 2004, 2017; Bright and Coleman 2001, 2003; Rose et al. 2018, 2021). Also, we considered the 1 km resolution Human Footprint (HFI, hereafter) dataset (Mu et al. 2022), which is expressed into eight different human pressure variables. These correspond to the intensity of human activities from 2000 to 2018, associated with built-up environments, population density, night-time lights, croplands, pastures, roads, railways, and navigable waterways.

Ultimately, to understand the temporal change trends and possible impacts of forest and settlement areas in the considered basins, we used the land cover data accessed from The Copernicus Climate Change Service (C3S). This is a 300 m resolution product referred to as Climate Data Store (CDS), generated by the European Space Agency (ESA) Climate Change Initiative (CCI). It summarized Land Cover (LC) data from 1992 to 2015 (Defourny et al. 2017) and Climate Data Records (ICDR) Land Cover data from 2016 to 2020 (Defourny et al. 2021). Notably, ICDR LC data from 2016 to 2020 are consistent with the ESA CCI LC data from 1992 to 2015 to ensure continuity (Defourny et al. 2021).

3 Methods

3.1 Data pre-processing

We prepared two different landslide datasets corresponding to (i) landslides triggered by natural factors (LTNF; i.e., precipitation) and (ii) landslides triggered by anthropogenic factors (LTAF; i.e., construction, mining activities, hill cutting, and other human activities).

Using the information on the geolocation accuracy, we created a buffer zone around each fatal landslide of 10 km. We then selected all sub-basins intersecting these buffers and represented landslide locations by them. This procedure was repeated for LTNF and LTAF. This has led to a total of 6744 sub-basins intersected by LTNF and 2081 sub-basins hosting LTAF.

While aggregating landslide information over sub-basins, we also aggregated corresponding environmental characteristics. The first aggregation step applies to the continuous characteristics. We calculated the mean values of (i) elevation, (ii) slope, (iii) elev-std, (iv) CTI, (v) precipitation, (vi) the annual rate of change for HFI, and vii) population. Furthermore, we computed the total population and calculated the trend of forest and settlement planimetric extents from land cover data.

We utilized Kernel Density Estimation (KDE, Silverman 1986) to define hotspots worldwide. First, we merged the LTNF and LTAF sub-basins and converted them to points. Next, we computed KDE within a moving window of a 100 km radius to obtain a continuous density surface. We then defined hotspots along the spatially coherent density surfaces by considering topographic and climatic characteristics. Moreover, to determine the landslide density for each sub-basin, we computed the KDE within a moving window with a radius of 10 km. Each sub-basin was then assigned with a fatal landslide density value corresponding to the mean of the KDE grid cells ($KDE_{sub\text{-}basin}$). The total population in each sub-basin ($Pop_{sub\text{-}basin}$) was also produced. This information allowed us to obtain the normalized landslide density (NLD) as the proportion of the last two parameters:

$$NLD = \frac{KDE_{sub-basin}}{Pop_{sub-basin}}$$

3.2 Bivariate spatial descriptors

Traditionally, maps represent the variation of a given parameter across the geographic space. Because the aim of this work is to examine the contextual effect of multiple parameters and check whether they can be used as discriminant tools between natural and

anthropogenic fatal landslides, we opted for an exploratory step based on bivariate maps. These are maps where the distribution of two parameters is grouped into a finite number of classes, and the combination of the two is then plotted via a two-dimensional color bar (Trumbo 1981; Robertson and O'Callaghan 1986). We initially applied this graphical technique to combine the spatial signals of the Köppen-Geiger climate classification together with a macro landform representation. Then, the frequency of LTNF and LTAF is calculated for each of the combined classes mentioned above. We also repeated the same operation for the two types of fatal landslides falling in a combined classification map showing landslide fatalities and their relative spatiotemporal persistence.

Moreover, we also computed the summary statistics of topographic, climatic, and anthropogenic proxies for each fatal landslide type. This information is summarized in a suite of scientific illustrations from which we base our interpretation and further discussions.

4 Results

4.1 Bivariate analysis

We examined the spatial distribution of selected fatal landslides over various climatic and landform conditions (Fig. 1a). We presented landslides triggered by natural and anthropogenic factors in Fig. 1b, c, respectively. After filtering out landslide locations due to the economic (GPD > $20,000) and spatial accuracy (> 10 km) criteria mentioned above, the resultant GFLD dataset has 2231 landslides, 1886 LTNF resulting in 18,301 deaths, and 345 LTAF causing 1162 deaths.

We initially looked into fatal landsliding per climatic and macro landform classes separately.

The major landslide concentration occurs around tropical (A, see Fig. 1) and temperate (C) regions quite similarly for both LTNF (A: 49.7% and C: 44.3%) and LTAF (A: 50.4% and C: 37.7%), respectively (see Table S1). In terms of fatalities, the highest number is also recorded in the tropical and temperate climatic regions for both LTNF (A: 52.1% and C: 34.7%) and LTAF (A: 52.7% and C: 35.5%), respectively. However, the lowest number is recorded in different climatic regions. The lowest fatalities for LTNF are associated with continental regions (D: 2.8%), whereas for LTAF, polar regions constitute the lowest incidences (E: 0.2%).

As for the landform categories, both the number of landslides and fatalities have the highest amount in low and middle mountains for LTNF (62.5% and 63.4%) and LTAF (41.4% and 43.2%), respectively (see Table S2). Notably, LTAF are about 20% lower than their naturally occurring counterparts regarding both the number of landslides and fatalities. This 20% difference appears as an increase in LTAF occurred in the plains and thus, both the number of LTAF and fatalities caused by them are approximately 20% higher compared to naturally occurring landslides.

The summary provided above is also presented in Fig. 2 through a combined climate-landform vision of fatal landsliding (Table S3). Figure 2 shows the frequency distribution of fatal landslides (stacked barplot) and fatalities per landslide (bubble plot) following the same color scheme of the bivariate climate-landform maps presented in Fig. 1. Panel (a) reports a graphical summary for LTNF, whereas panel (b) shows the situation for LTAF.

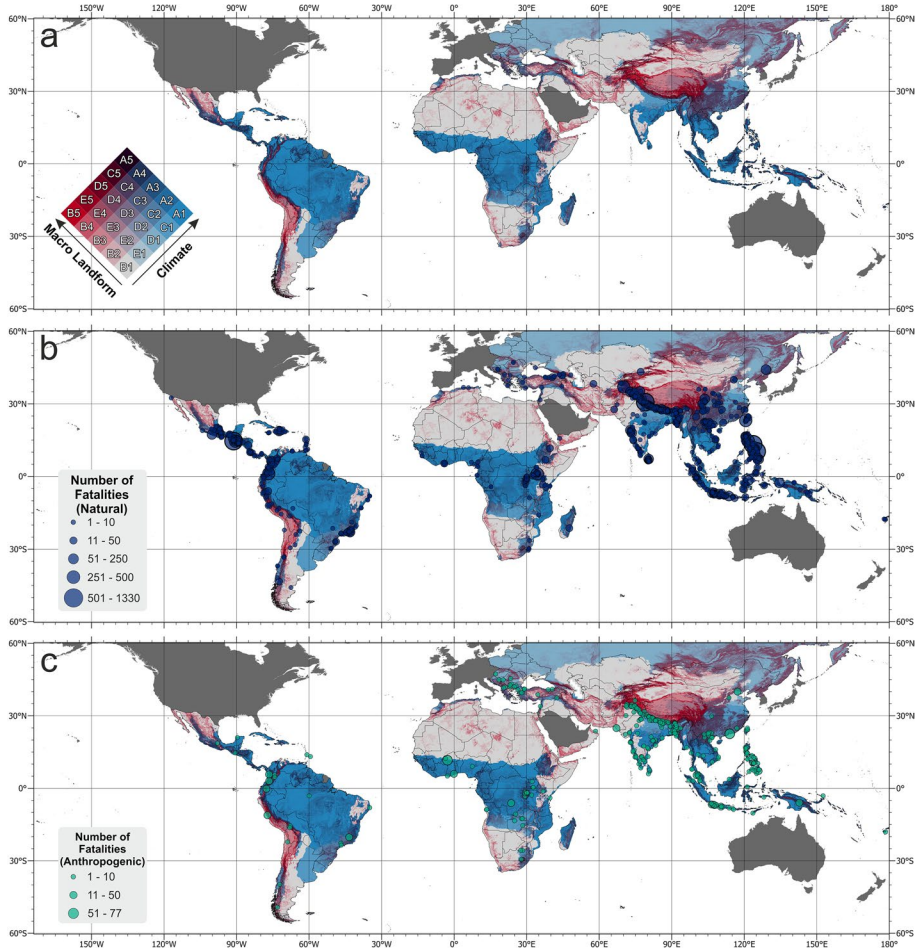

Fig. 1 Panels showing **a** the climate-landform combined map and the same map overlaid by the spatial distribution of fatal landslides and fatalities triggered by **b** natural and **c** anthropogenic factors. Climatic information is based on (A) tropical, (B) arid, (C) temperate, (D) continental, and (E) polar regions. The macro landform information is expressed into plains (1), lowlands, platforms, and low plateaus (2), middle, high, and very high plateaus (3), low and middle mountains (4), and high and very high mountains (5). The size of the landslide point indicates the number of fatalities for each event. Grey areas indicate regions that were masked out

Overall, our analyses show that mountainous areas of tropical and temperate climatic regions appear to be the main concentration areas of LTNF and cause considerable life losses. A similar situation with some slight differences also appears for LTAF. Specifically, they mostly concentrate around mountainous areas of tropical and temperate climatic regions as seen for natural ones. The difference is that LTAF are also located in plains of tropical and temperate climatic regions. We also note that mortality rates (i.e., average number of fatalities per landslide) are much higher for naturally triggered landslides than anthropogenically induced ones (Fig. 2).

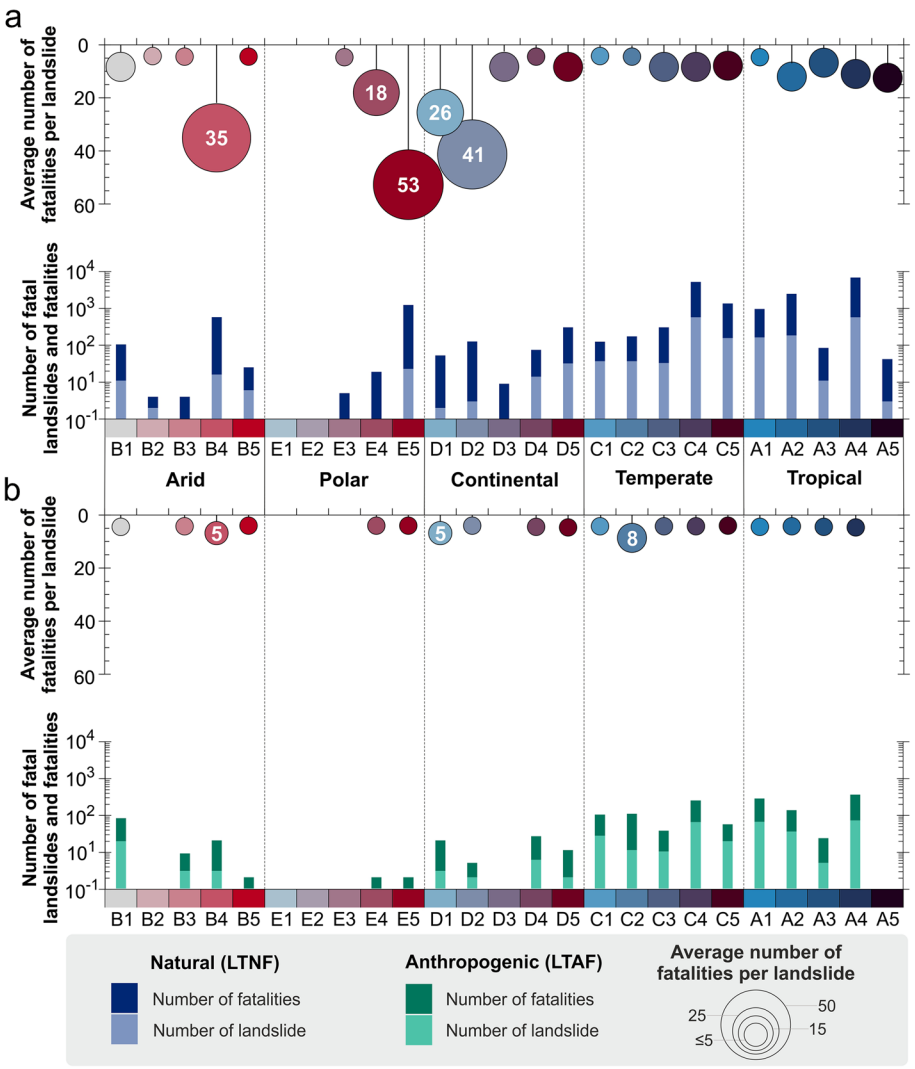

Fig. 2 Climate-landform regions vary in the number of fatal landslides and fatalities (bottom panel) triggered by **a** natural triggering and **b** anthropogenic triggering factors (in log-scale). The bubble plots (top panel) in (**a**) and (**b**) show the average number of fatalities per landslide (FpL). (see Fig. 1a and Table S3 for a description of the climate-landform classification)

Figure 3 shows persistence and the total number of incidences (i.e., landslides or fatalities) over sub-basins. The total number of landslides or the total number of fatalities associated with a given sub-basin is referred to as incidence. We define persistence, on the other hand, in relation to the recurrence of landsliding for a given sub-basin. A higher persistence indicates a larger number of landslides occurring over time in a sub-basin.

For LTNF, Fig. 3a summarizes this information in bivariate plots showing both the incidence (where the maximum value is 14) and their persistence (where the maximum value is 9) together. Figure 3b presents the same information but shows the number of victims

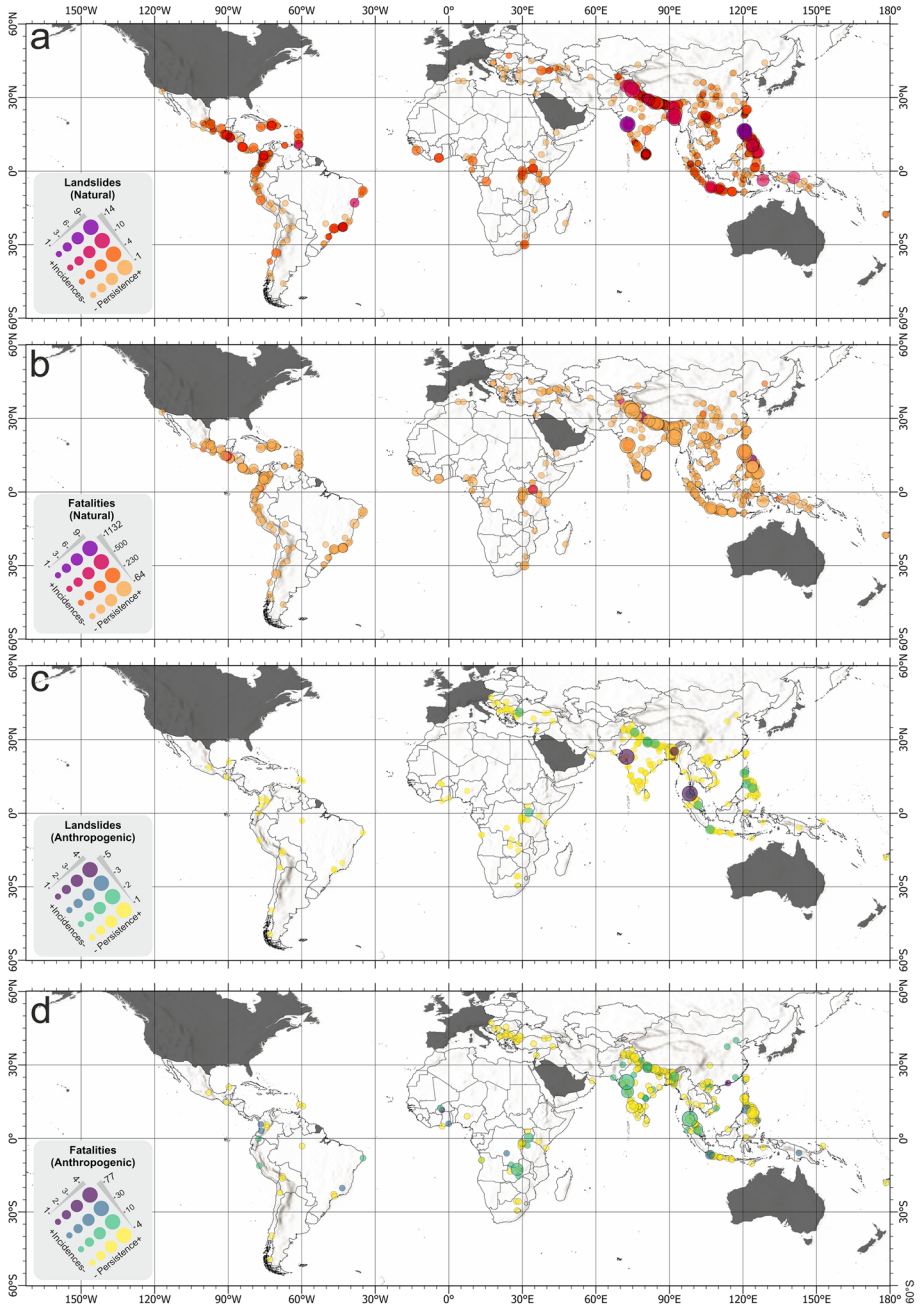

Fig. 3 The maps illustrate the spatial persistence of **a** landslides and **b** associated due to natural factors, as well as **c** landslides and **d** fatalities due to anthropogenic factors. The darker the color of the bubbles representing the sub-basins, the higher the number of landslides and fatalities, and the larger their size, the higher the persistence

per sub-basin and their persistence (where the maximum values are 1132 and 9, respectively). The same is reported in Fig. 3c, d for LTAF.

Results show that South and Southeast Asia host sub-basins characterized by the highest incidences and persistence for fatal landslides triggered by natural agents. Sub-basins located in this region have a maximum of 14 landslides (i.e., high incidence) that occurred on up to nine different occasions (i.e., high persistence). Central and South America show a relatively high landslide incidence (the maximum value is 7), with a persistence of up to three occurrences (Fig. 3a).

A similar spatial pattern arises when looking at fatalities from the same incidence-persistence perspective (Fig. 3b), with a slight difference associated with incidences. Notably, landslides with many fatalities are relatively rare, which is why high incidences are rarely coupled by high persistence.

The sub-basins with the highest incidences characterized by the high persistence for landslides (Fig. 3c) and fatalities (Fig. 3d) associated with anthropogenic agents are also located in South and Southeast Asia. As seen in the naturally occurring landslides, events with a high number of fatalities are also rare in this case.

To further explore the link between incidence and persistence for the examined sub-basins, we created scatter plots (Fig. 4) for incidence and persistence for each climate-landform class. Results show that in general, sub-basins exposed to fatal landslides experience these events repetitively. Specifically, tropical and temperate climatic areas host sub-basins where fatal landslides occur repeatedly and thus, Fig. 4 indicates high persistence in those regions. Continental, polar, and arid areas, on the other hand, are dominantly characterized by low persistence.

4.2 Controlling factors analysis

This section presents the summary statistics of basin characteristics that host LTNF or LTAF (Fig. 5). To avoid repeated information, we exclude basins hosting both LTNF and LTAF.

Topographically, LTNF has a higher elevation, elev-std, and slope median values compared to the LTAF. The median values for LTNF are 724.2 m, 17.8 m, and 11.3°, respectively. As for LTAF, the median values are 372.0 m, 5.7 m, and 3.6°, respectively. A difference can also be seen in the long-term average annual precipitation, albeit less pronounced as compared to the morphometric cases. Specifically, LTNF has an annual precipitation centered at 2145 mm, while it is 1499 mm for LTAF. As for the total population, the median value is much higher for LTAF (27,167) as compared to LTNF (16,530).

5 Discussion

Our results show that LTNF is associated with higher average fatality rates than LTAF, specifically in arid, polar, and continental climatic regions when we consider the average number of fatalities per climate-landform region (see Fig. 2). This indicates that LTNF are much rarer in these environments, although the rate of mortality per single landslide is also much higher. Conversely, LTNF are much more common in tropical and temperate climatic regions (94% of the total) but their mortality rate is comparably lower than in other regions. However, when we examine fatalities at the sub-basic level, results show that high fatalities are mostly associated with rare landslides (see Fig. 4).

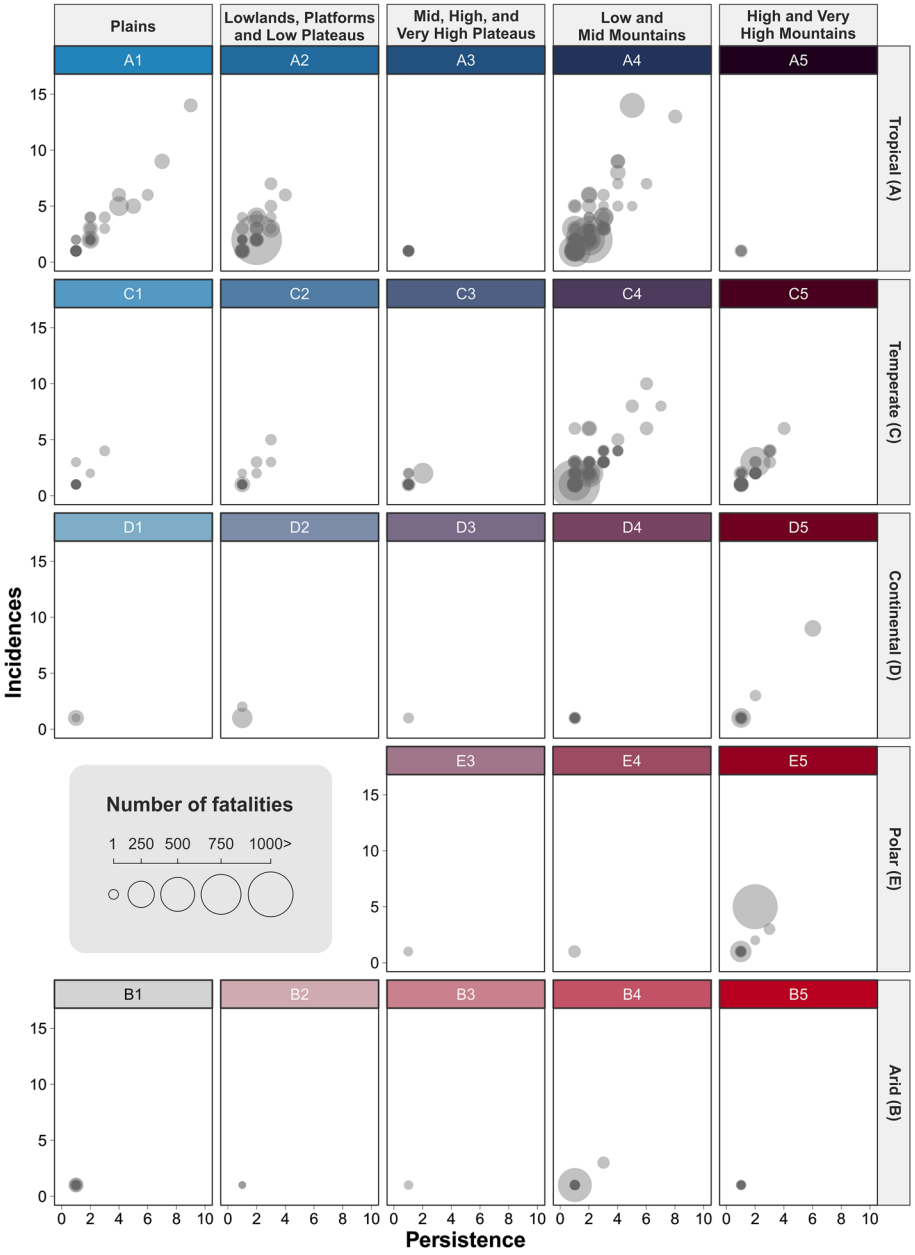

Fig. 4 Panels showing persistence vs incidences of fatal landslides over different climate-landform regions

We computed spatial densities to complement the information presented above (Fig. 6). The fatal landslides across the Himalayan Range are shown separately because they would saturate the signal due to the large number of samples from this rough terrain.

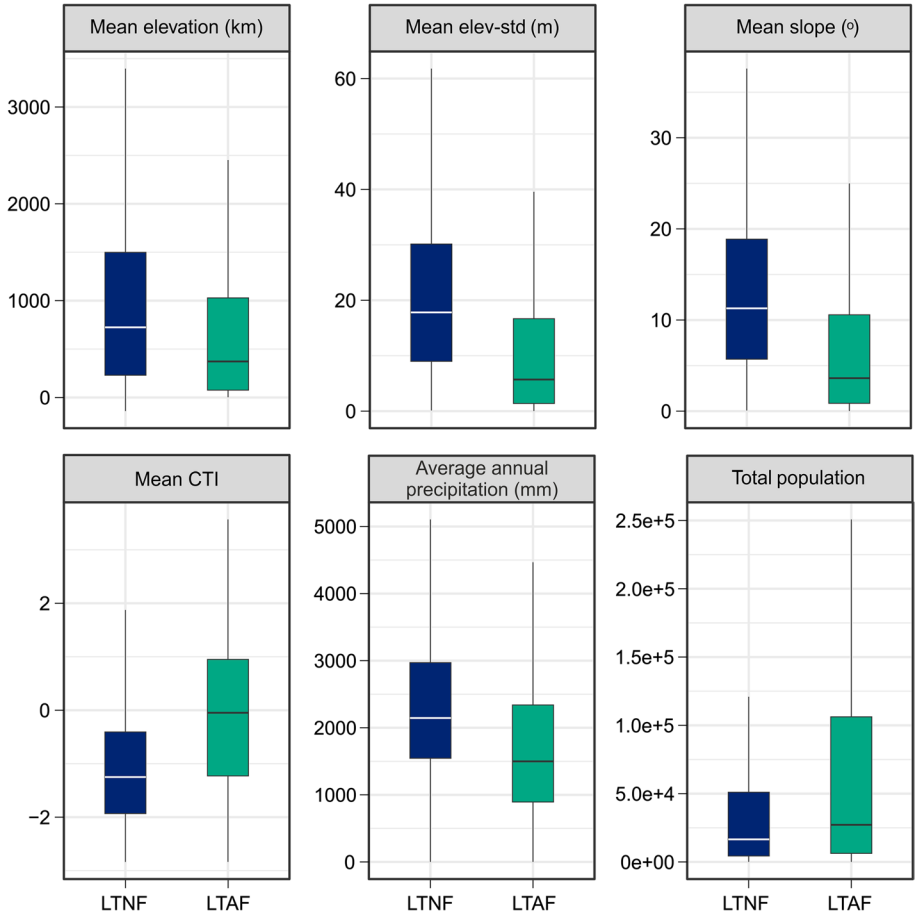

Fig. 5 Graphs showing the distribution of different controlling factors of fatal landslides are presented separately for both LTNF (blue boxplots) and LTAF (green boxplots)

Based on landslide densities, we identified ten hotspots distributed in Central American Ranges and Hispaniola, Northern Andes, Brazilian Highlands, Great Rift Valley, Western Ghats and Sri Lanka, Himalayan Range, North East India and Bangladesh, Vietnam, Philippines and Taiwan, and Indonesia (Fig. 6). These regions also refer to areas where landslide rates are expected to increase due to climate change. By the end of this century, as global mean surface temperature increases, extreme precipitation events over most of the mid-latitude land masses and over wet tropical regions will very likely become more intense and more frequent (IPCC 2014). As a result, for instance, shallow landslides and debris flows are expected to increase because of extreme weather events in South and Southeast Asia, Central America and South America, and the Great Rift Valley (Gariano and Guzzetti 2016) and Himalayan range (Kirschbaum et al. 2020). Also, La Nina conditions, which lead to greater landslide exposure, are projected to show the most significant increases in northern South America, Central America and the Caribbean, Indonesia, and the Philippines (Emberson et al. 2021). When land degradation caused by increased human disturbance is added to this, a worse picture may emerge.

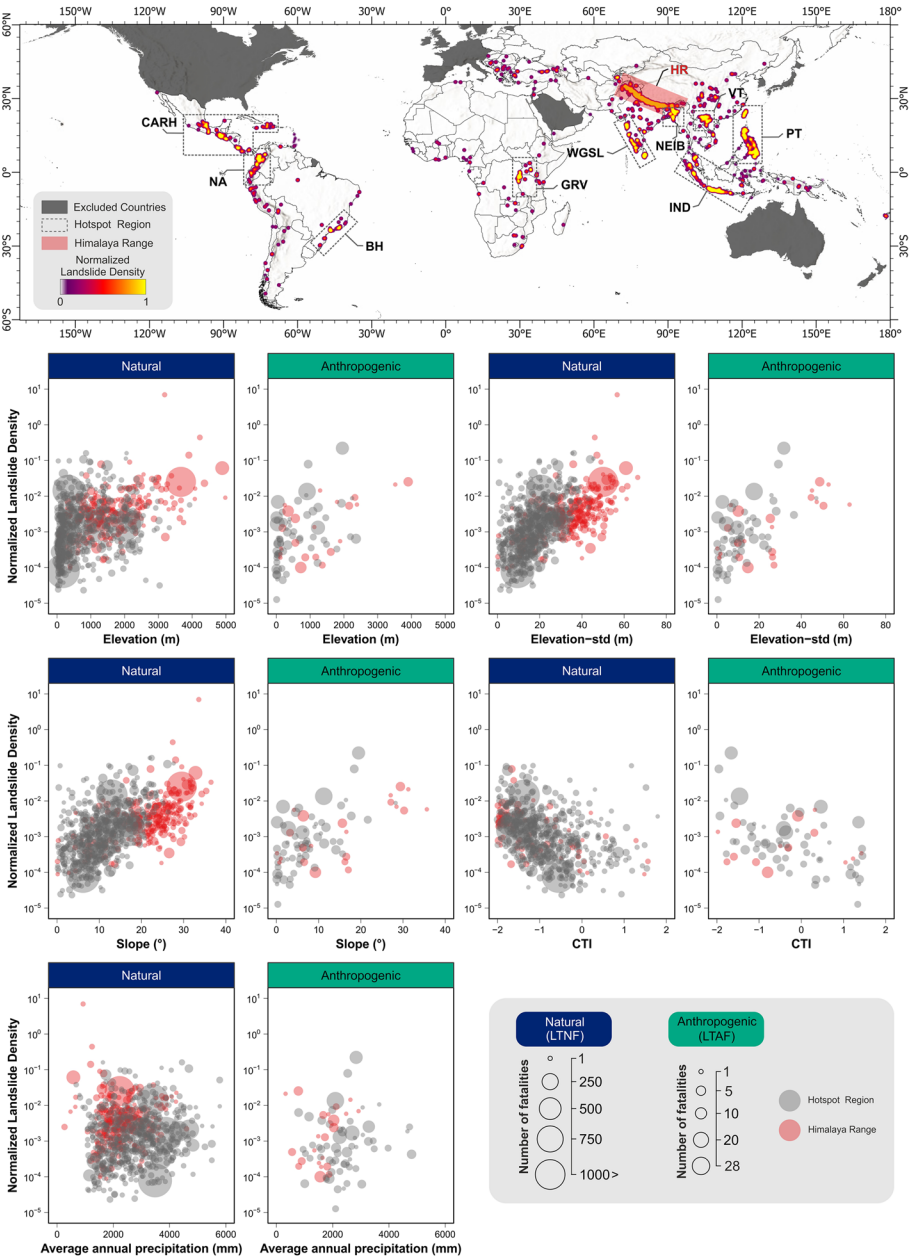

Fig. 6 The map shows sub-basin hotspots representing fatal landslides triggered by natural and anthropogenic factors. In the map, the grey dashed line section represents hot spot areas: Central American Ranges and Hispaniola (CARH), Northern Andes (N.A.), Brazilian Highlands (B.H.), Great Rift Valley (GRV), Western Ghats and Sri Lanka (WGSL), Himalayan Range (H.R.), North East India and Bangladesh (NEIB), Vietnam (V.T.), Philippines and Taiwan (P.T.), Indonesia (IND). See Fig. S1 for a zoomed-in representation of the hot spot areas. The graphs plot the distributional characteristics of normalized landslide density (NLD) and fatalities according to the factors controlling landslides. NLD represents the landslide density ($KDE_{sub\text{-}basin}$) in each sub-basin divided by the number of people ($Pop_{sub\text{-}basin}$)

The LTNF and LTAF densities demonstrate a positive correlation with elevation, elev-std, and steepness and a negative correlation with CTI, as expected (Fig. 6). No discernible pattern arises in the average annual precipitation, which is somewhat counter-intuitive, but may reflect the adaptation of the landscape to the prevailing climatic conditions. Aside from a few exceptions, LTNF generates more fatalities, these being mostly localized up in the topographic profile at 1019.3 m a.s.l., whereas the same occurs for LTAF at 666 m a.s.l.

Interestingly, the fatal landslides occur at higher elevations on steeper hillslopes in the Himalayan range as compared to the rest of the dataset (Fig. 6). This is mainly because of the population in the Himalayan range at high elevations. Landslides triggered by natural factors may of course have been influenced by anthropogenic factors because human activities can lead to reduced hillslope stability, which may not be directly seen in this dataset.

Our results also indicate that fatal landslides triggered by natural and anthropogenic factors differ in terms of topography, precipitation, and population density characteristics. LTNF occurs at a much higher elevation, elev-std, slope, and rainfall conditions. These correspond to regions where the population is relatively low compared to its anthropogenic counterpart (see Fig. 5). Considering that 74.2% of LTNF occur in mountainous areas (Table S2), these landslides result in more fatalities and higher impacts despite the lower population density because these landslides are predominantly triggered by prolonged or extreme rainfall that typically affects larger areas. In contrast, LTAF are extremely localized over densely populated areas due to human intervention. Since these landslides usually occur in urban areas and mining sites (Froude and Petley 2018), their topographic characteristics differ from those of LTNF.

Capturing the possible role of anthropogenic factors in the occurrence of naturally triggered landslides is a challenge because human impact may occur over long time periods, which are hard to unfold (Glade 2003; Guns and Vanacker 2014; Depicker et al. 2021). Rather than focusing on different environmental conditions characterizing naturally and anthropogenically induced landslides, identifying similarities between these two could be another way to approach this discussion. We do so by examining the role of land cover change and increasing human pressure in connection to both LTNF and LTAF locations. Figure 7 shows that in both cases, we observe quite similar trends in changes in forest cover and proxies of human impact. This implies that human impact disturbing hillslope stabilities in the case of anthropogenically triggered landslides may also exist for naturally occurring ones. Further research on this issue with higher resolution and reliable data is needed. Based on these results, we suggest that anthropogenic factors may also have a partial role in naturally occurring landslides.

6 Conclusions

This study provides insight into the spatially persistent pattern of fatal landslides in relation to topographic and climatic factors likely controlling landslide occurrences. Our analyses indicate that landslides triggered by natural factors (69.3%) and fatalities (66.7%), as well as landslides triggered by anthropogenic factors (44.1%) and fatalities (43.0%), occur most frequently in the mountains and tropical/temperate climatic regions.

We also showed that LTNF tends to occur at higher elevations on steeper slopes, while LTAF concentrates at lower elevations and gentler slopes. South and Southeast Asia, Central America and South America, and the Great Rift Valley are global-scale hotspots of fatal landslides. These hotspots correspond to areas vulnerable to climate

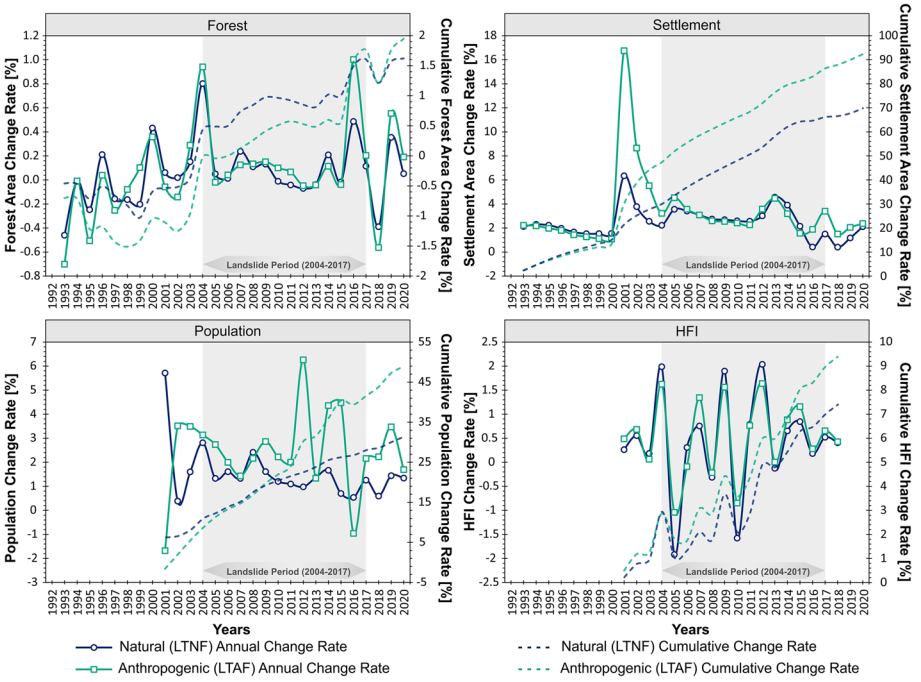

Fig. 7 Temporal variations in forest area, settlement area, population and human footprint changes in sub-basins associated with LTNF (blue) and LTAF (green). The solid lines indicate the annual change rate, whereas the dashed lines represent the cumulative change rate

change and, thus, landscapes with an expected increase in landsliding rates. Therefore, these susceptible areas could be more vulnerable in the future when climatic extremes are coupled with human impact.

Our research also highlights the role of land cover changes and increased human pressure in the occurrence of natural-induced fatal landslides. In this context, we argue that human activities impact not only fatal landslides of anthropogenic origin but also fatal landslides of natural origin. In this respect, we emphasize the importance of understanding the complex interactions between natural and human factors in the occurrence of fatal landslides. Comprehensive and adaptive strategies are needed to reduce landslide risks in mountainous areas of tropical and temperate climatic regions, especially in the face of climate change and increasing human pressure. Finally, future work should continue to monitor and assess fatal landslides and focus on developing more reliable and comprehensive inventories.

Supplementary Information The online version contains supplementary material available at https://doi.org/10.1007/s11069-024-06487-3.

Acknowledgements Seçkin Fidan is grateful to the Scientific and Technological Research Council of Turkey (TÜBİTAK), International Research Fellowship Programme for Doctoral Students (BİDEB 2214-A). Seçkin Fidan would like to express his sincere thanks to the Faculty of Geo-Information Science and Earth Observation (ITC), Department of Applied Earth Sciences (AES), for hosting him as a visiting PhD student. The authors thank Abdüssamet Yılmaz for his support during the analysis process.

Funding Open access funding provided by the Scientific and Technological Research Council of Türkiye (TÜBİTAK). This work was supported by the Istanbul Technical University (ITU) Scientific Research Projects Coordination Unit (Project No: MDK-2021-43288 for Ph.D. Thesis).

Declarations

Conflict of interest The authors declare no competing interests.

References

Alexander D (2005) Vulnerability to landslides. In: Glade T, Anderson MGCM (eds) Landslide hazard and risk. Wiley, Chichester, pp 175–198

Amatulli G, McInerney D, Sethi T et al (2020) Geomorpho90m, empirical evaluation and accuracy assessment of global high-resolution geomorphometric layers. Sci Data 7:1–18. https://doi.org/10.1038/s41597-020-0479-6

Beck HE, Zimmermann NE, McVicar TR et al (2018) Present and future Köppen–Geiger climate classification maps at 1-km resolution. Sci Data 5:1–12. https://doi.org/10.1038/sdata.2018.214

Bright E, Coleman P (2001) LandScan Global 2000. Oak Ridge National Laboratory SE - July 01, Oak Ridge, TN. https://doi.org/10.48690/1524196

Bright E, Coleman P (2002) LandScan Global 2001. Oak Ridge National Laboratory SE—July 01, Oak Ridge, TN. https://doi.org/10.48690/1524197

Bright E, Coleman P (2003) LandScan Global 2002. Oak Ridge National Laboratory SE - July 01, Oak Ridge, TN. https://doi.org/10.48690/1524198

Bright E, Coleman P, King A (2004) LandScan Global 2003. Oak Ridge National Laboratory SE - July 01, Oak Ridge, TN. https://doi.org/10.48690/1524199

Bright E, Coleman P, King A (2005) LandScan Global 2004. Oak Ridge National Laboratory SE - July 01, Oak Ridge, TN. https://doi.org/10.48690/1524200

Bright E, Coleman P, King A (2006) LandScan Global 2005. Oak Ridge National Laboratory SE - July 01, Oak Ridge. https://doi.org/10.48690/1524201

Bright E, Coleman P, King A (2007) LandScan Global 2006. Oak Ridge National Laboratory SE - July 01, Oak Ridge, TN. https://doi.org/10.48690/1524202

Bright E, Coleman P, King A, Rose A (2008) LandScan Global 2007. Oak Ridge National Laboratory SE - July 01, Oak Ridge, TN. https://doi.org/10.48690/1524203

Bright E, Coleman P, King A, Rose A, Urban M (2009) LandScan Global 2008. Oak Ridge National Laboratory SE - July 01, Oak Ridge, TN. https://doi.org/10.48690/1524204

Bright E, Coleman P, Rose A, Urban M (2010) LandScan Global 2009. Oak Ridge National Laboratory SE - July 01, Oak Ridge, TN. https://doi.org/10.48690/1524205

Bright E, Coleman P, Rose A, Urban M (2011) LandScan Global 2010. Oak Ridge National Laboratory SE - July 01, Oak Ridge, TN. https://doi.org/10.48690/1524206

Bright E, Coleman P, Rose A, Urban M (2012) LandScan Global 2011. Oak Ridge National Laboratory SE - July 01, Oak Ridge, TN. https://doi.org/10.48690/1524207

Bright E, Rose A, Urban M (2013) LandScan Global 2012. Oak Ridge National Laboratory SE - July 01, Oak Ridge, TN. https://doi.org/10.48690/1524215

Bright E, Rose A, Urban M (2014) LandScan Global 2013. Oak Ridge National Laboratory SE - July 01, Oak Ridge, TN. https://doi.org/10.48690/1524208

Bright E, Rose A, Urban M (2015) LandScan Global 2014. Oak Ridge National Laboratory SE - July 01, Oak Ridge, TN. https://doi.org/10.48690/1524209

Bright E, Rose A, Urban M (2016) LandScan Global 2015. Oak Ridge National Laboratory SE - July 01, Oak Ridge, TN. https://doi.org/10.48690/1524210
Bright E, Rose A, Urban M, McKee J (2017) LandScan Global 2016. Oak Ridge National Laboratory SE - July 01, Oak Ridge, TN. https://doi.org/10.48690/1524211
Climate Data Store (2019) Land cover classification gridded maps from 1992 to present derived from satellite observations. Copernicus Climate Change Service. 7–9
Defourny P, Lamarche C, Bontemps S, De Maet T, Van Bogaert E, Moreau I, Brockmann C, Boettcher M, Kirches G, Wevers J, Santoro M, Ramoino F, Arino O (2017) Land cover climate change initiative—product user guide v2. Issue 2.0
Defourny P, Lamarche C, Marissiaux Q, Carsten B, Martin B, Grit K (2021) Product user guide and specification, ICDR Land Cover 2016–2020
Depicker A, Jacobs L, Mboga N et al (2021) Historical dynamics of landslide risk from population and forest-cover changes in the Kivu Rift. Nat Sustain. https://doi.org/10.1038/s41893-021-00757-9
Emberson R, Kirschbaum D, Amatya P et al (2022) Insights from the topographic characteristics of a large global catalog of rainfall-induced landslide event inventories. Nat Hazards Earth Syst Sci Discuss 22:1129–1149
Emberson R, Kirschbaum D, Stanley T (2021) Global connections between El Nino and landslide impacts. Nat Commun 12:1–11. https://doi.org/10.1038/s41467-021-22398-4
Froude MJ, Petley DN (2018) Global fatal landslide occurrence from 2004 to 2016. Nat Hazards Earth Syst Sci 18:2161–2181. https://doi.org/10.5194/nhess-18-2161-2018
Garcia-Delgado H, Petley DN, Bermúdez MA, Sepúlveda SA (2022) Fatal landslides in Colombia (from historical times to 2020) and their socio-economic impacts. Landslides 19:1689–1716. https://doi.org/10.1007/s10346-022-01870-2
Gariano SL, Guzzetti F (2016) Landslides in a changing climate. Earth-Sci Rev 162:227–252. https://doi.org/10.1016/j.earscirev.2016.08.011
Glade T (2003) Landslide occurrence as a response to land use change: a review of evidence from New Zealand. CATENA 51:297–314. https://doi.org/10.1016/S0341-8162(02)00170-4
Görüm T, Fidan S (2021) Spatiotemporal variations of fatal landslides in Turkey. Landslides 18:1691–1705. https://doi.org/10.1007/s10346-020-01580-7
Grima N, Edwards D, Edwards F et al (2020) Landslides in the Andes: forests can provide cost-effective landslide regulation services. Sci Total Environ 745:141128. https://doi.org/10.1016/j.scitotenv.2020.141128
Guns M, Vanacker V (2014) Shifts in landslide frequency-area distribution after forest conversion in the tropical Andes. Anthropocene 6:75–85. https://doi.org/10.1016/j.ancene.2014.08.001
Haque U, Blum P, da Silva PF et al (2016) Fatal landslides in Europe. Landslides 13:1545–1554. https://doi.org/10.1007/s10346-016-0689-3
Haque U, da Silva PF, Devoli G et al (2019) The human cost of global warming: deadly landslides and their triggers (1995–2014). Sci Total Environ 682:673–684. https://doi.org/10.1016/j.scitotenv.2019.03.415
IPCC—Intergovernmental Panel on Climate Change (2014) Climate Change 2014: synthesis Report. Contribution of Working Groups I, II and III to the Fifth Assessment Report of the Intergovernmental Panel on Climate Change. Geneva, Switzerland
Karger DN, Conrad O, Böhner J et al (2017) Climatologies at high resolution for the earth's land surface areas. Sci Data 4:1–20. https://doi.org/10.1038/sdata.2017.122
Karger DN, Wilson AM, Mahony C et al (2021) Global daily 1 km land surface precipitation based on cloud cover-informed downscaling. Sci Data 8:1–18. https://doi.org/10.1038/s41597-021-01084-6
Kirschbaum D, Adler R, Adler D et al (2012) Global distribution of extreme precipitation and high-impact landslides in 2010 relative to previous years. J Hydrometeorol 13:1536–1551. https://doi.org/10.1175/JHM-D-12-02.1
Kirschbaum D, Kapnick SB, Stanley T, Pascale S (2020) Changes in extreme precipitation and landslides over high mountain asia. Geophys Res Lett 47:1–9. https://doi.org/10.1029/2019GL085347
Kirschbaum D, Stanley T, Zhou Y (2015) Spatial and temporal analysis of a global landslide catalog. Geomorphology 249:4–15. https://doi.org/10.1016/j.geomorph.2015.03.016
Kirschbaum DB, Adler R, Hong Y et al (2010) A global landslide catalog for hazard applications: method, results, and limitations. Nat Hazards 52:561–575. https://doi.org/10.1007/s11069-009-9401-4
Lehner B, Grill G (2013) Global river hydrography and network routing: baseline data and new approaches to study the world's large river systems. Hydrol Process 27:2171–2186. https://doi.org/10.1002/hyp.9740
Lin Q, Wang Y (2018) Spatial and temporal analysis of a fatal landslide inventory in China from 1950 to 2016. Landslides 15:2357–2372. https://doi.org/10.1007/s10346-018-1037-6

Maki Mateso JC, Bielders CL, Monsieurs E et al (2023) Characteristics and causes of natural and human-induced landslides in a tropical mountainous region: the rift flank west of Lake Kivu (Democratic Republic of the Congo). Nat Hazards Earth Syst Sci 23:643–666. https://doi.org/10.5194/nhess-23-643-2023

Meybeck M, Green P, Vörösmarty C (2001) A new typology for mountains and other relief classes. Mt Res Dev 21:34–45. https://doi.org/10.1659/0276-4741(2001)021[0034:antfma]2.0.co;2

Mu H, Li X, Wen Y et al (2022) A global record of annual terrestrial Human Footprint dataset from 2000 to 2018. Sci Data 9:1–9. https://doi.org/10.1038/s41597-022-01284-8

Ozturk U, Bozzolan E, Holcombe EA et al (2022) How climate change and unplanned urban sprawl bring more landslides. Nature 608:262–265. https://doi.org/10.1038/d41586-022-02141-9

Petley D (2012) Global patterns of loss of life from landslides. Geology 40:927–930. https://doi.org/10.1130/G33217.1

Petley DN (2010) On the impact of climate change and population growth on the occurrence of fatal landslides in South, East and SE Asia. Q J Eng Geol Hydrogeol 43:487–496. https://doi.org/10.1144/1470-9236/09-001

Petley DN, Hearn ÆGJ, Hart ÆA, et al (2007) Trends in landslide occurrence in Nepal. 23–44. https://doi.org/10.1007/s11069-006-9100-3

Robertson PK, O'Callaghan JF (1986) The generation of color sequences for univariate and bivariate mapping. IEEE Comput Graph Appl 6:24–32. https://doi.org/10.1109/MCG.1986.276688

Rose A, McKee J, Sims K, et al (2020) LandScan Global 2019

Rose A, McKee J, Sims K, et al (2021) LandScan Global 2020

Rose A, McKee J, Urban M, et al (2019) LandScan Global 2018

Rose A, McKee J, Urban M, Bright E (2018) LandScan Global 2017

Sepúlveda SA, Petley DN (2015) Regional trends and controlling factors of fatal landslides in Latin America and the Caribbean. Nat Hazards Earth Syst Sci 15:1821–1833. https://doi.org/10.5194/nhess-15-1821-2015

Silverman BW (1986) Density estimation for statistics and data analysis. CRC Press, Boca Raton

Tanyaş H, van Westen CJ, Allstadt KE et al (2017) Presentation and analysis of a worldwide database of earthquake-induced landslide inventories. J Geophys Res Earth Surf 122:1991–2015. https://doi.org/10.1002/2017JF004236

Trumbo BE (1981) A theory for coloring bivariate statistical maps published by: Taylor & Francis, Ltd. on behalf of the American Statistical Association Stable. http://www.jstor.org/stable/2683294 All use subject to http://about.jstor.org/terms A Theory for Colori. Am Stat 35:220–226

World Bank (2017) GDP per capita (current US$)

Yamazaki D, Ikeshima D, Tawatari R et al (2017) A high-accuracy map of global terrain elevations. Geophys Res Lett 44:5844–5853. https://doi.org/10.1002/2017GL072874